

₁ Study of neutrino-nucleus interaction at around 1 GeV using
₂ a 3D grid-structure neutrino detector, WAGASCI, muon
₃ range detectors and magnetized spectrometer, Baby MIND,
₄ at J-PARC neutrino monitor hall

₅ A. Bonnemaison, R. Cornat, L. Domine, O. Drapier, O. Ferreira, F. Gastaldi,
₆ M. Gonin, J. Imber, M. Licciardi, F. Magniette, T. Mueller, L. Vignoli, and O. Volcy
₇ *Ecole Polytechnique, IN2P3-CNRS, Laboratoire Leprince-Ringuet, Palaiseau,*
₈ *France*

₉ S. Cao and T. Kobayashi

₁₀ *High Energy Accelerator Research Organization (KEK), Tsukuba, Ibaraki, Japan*

₁₁ M. Khabibullin, A. Khotjantsev, A. Kostin, Y. Kudenko, A. Mefodiev, O. Mineev,
₁₂ S. Suvorov, and N. Yershov

₁₃ *Institute for Nuclear Research of the Russian Academy of Sciences, Moscow, Russia*

₁₄ B. Quilain

₁₅ *Kavli Institute for the Physics and Mathematics of the Universe (WPI), The*
₁₆ *University of Tokyo Institutes for Advanced Study, University of Tokyo, Kashiwa,*
₁₇ *Chiba, Japan*

₁₈ T. Hayashino, A. Hiramoto, A.K. Ichikawa, K. Nakamura, T. Nakaya, K Yasutome,
₁₉ and K. Yoshida

₂₀ *Kyoto University, Department of Physics, Kyoto, Japan*

₂₁ Y. Azuma, J. Harada, T. Inoue, K. Kin, N. Kukita, S. Tanaka, Y. Seiya,
₂₂ K. Wakamatsu, and K. Yamamoto

₂₃ *Osaka City University, Department of Physics, Osaka, Japan*

²⁴ A. Blondel, F. Cadoux, Y. Favere, E. Noah, L. Nicola, and S. Parsa

²⁵ *University of Geneva, Section de Physique, DPNC, Geneva, Switzerland*

²⁶ N. Chikuma, F. Hosomi, T. Koga, R. Tamura, and M. Yokoyama

²⁷ *University of Tokyo, Department of Physics, Tokyo, Japan*

²⁸ Y. Hayato

²⁹ *University of Tokyo, Institute for Cosmic Ray Research, Kamioka Observatory,
30 Kamioka, Japan*

³¹ Y. Asada, K. Matsushita, A. Minamino, K. Okamoto, and D. Yamaguchi

³² *Yokohama National University, Faculty of Engineering, Yokohama, Japan*

³³ December 12, 2017

³⁴ 1 Introduction

³⁵ The understanding of neutrino-nucleus interactions in the 1 GeV energy region is critical
³⁶ for the success of accelerator-based neutrino oscillation experiments such as the T2K exper-
³⁷ iment. Complicated multi-body effects of nuclei render this understanding difficult. The
³⁸ T2K near detectors have been measuring these and significant progress has been achieved.
³⁹ However, the understanding is still limited. One of the big factors preventing from full
⁴⁰ understanding is the non-monochromatic neutrino beam spectrum. Measurements with
⁴¹ different but some overlapping beam spectra would greatly benefit to resolve the contri-
⁴² bution from different neutrino energies. We, the Wagasci collaboration, proposes to study
⁴³ the neutrino-nucleus interaction at the B2 floor of the neutrino monitor building, where
⁴⁴ different neutrino spectra can be obtained due to the different off-axis position. Our exper-
⁴⁵ imental setup contains 3D grid-structure plastic-scintillator detectors filled with water as
⁴⁶ the neutrino interaction target (Wagasci modules), two side- and one downstream- muon
⁴⁷ range detectors(MRD's). The 3D grid-structure and side-MRD's allows a measurement of
⁴⁸ wider-angle scattering than the T2K off-axis near detector (ND280). High water to scintil-
⁴⁹ lator material ratio enables the measurement of the neutrino interaction on water, which
⁵⁰ is highly desired for the T2K experiment because it's far detector, Super-Kamiokande,

51 is composed of water. The MRD's consist of plastic scintillators and iron plates. The
52 downstream-MRD, so called the Baby MIND detector, also works as a magnet and pro-
53 vides the charge identification capability as well as magnetic momentum measurement for
54 high energy muons. The charge identification is essentially important to select antineu-
55 trino events in the antineutrino beam because contamination of the neutrino events is as
56 high as 30%. Most of the detectors has been already constructed. The Wagasci modules
57 have been commissioned as the J-PARC T59 experiment and the Baby MIND detector was
58 commissioned at the CERN neutrino platform. Therefore, the collaboration will be ready
59 to proceed to the physics data taking for the T2K beam time in January 2019. We will
60 provide the cross sections of the charged current neutrino and antineutrino interactions on
61 water with slightly higher neutrino energy than T2K ND280 with wide angler acceptance.
62 When combined with ND280 measurements, our measurement would greatly improve the
63 understanding of the neutrino interaction at around 1 GeV and contribute to reduce one
64 of the most significant uncertainty of the T2K experiment.

65 **2 Experimental Setup**

66 Figure. 1 shows a schematic view of the entire set of detectors. A central detector, Wagasci
67 modules, consists of 3D grid-structure plastic-scintillator detectors filled with water as the
68 neutrino interaction target. They are surrounded by two side- and one downstream- muon
69 range detectors(MRD's) The MRD's are used to select muon tracks from the charged-
70 current (CC) interactions and to reject short tracks caused by neutral particles that orig-
71 inate mainly from neutrino interactions in material surrounding the central detector, like
72 the walls of the detector hall, neutrons and gammas, or neutral-current (NC) interactions.
73 The muon momentum can be reconstructed from its range inside the detector. The MRD's
74 consist of plastic scintillators and iron plates. In addition, each of the iron plates of the
75 downstream-MRD, so called the Baby MIND detector, is wound by a coil and can be
76 magnetized. It provide the charge selection capability.

77 For all detectors, scintillation light in the scintillator bar is collected and transported
78 to a photodetector with a wavelength shifting fiber (WLS fiber). The light is read out by
79 a photodetector, Multi-Pixel Photon Counter (MPPC), attached to one end of the WLS
80 fiber. The signal from the MPPC is read out by the dedicated electronics developed for the
81 test experiment to enable bunch separation in the beam spill. The readout electronics is
82 triggered using the beam-timing signal from MR to synchronize to the beam. The beam-
83 timing signal is branched from those for T2K, and will not cause any effect on the T2K
84 data taking.

85 T2K adopted the off-axis beam method, in which the neutrino beam is intentionally
86 directed 2.5 degrees away from SK producing a narrow band ν_μ beam. The off-axis near
87 detector, ND280, is installed towards the SK direction in the B1 floor of the near detector
88 hall of the J-PARC neutrino beam-line. We propose to install our detector in the B2 floor

tmp.pdf

Figure 1: Schematic view of entire sets of detectors.

89 of the near detector hall, where the off-axis angle is similar but slightly different: 1.5 degree.
90 The candidate detector position in the B2 floor is shown in Fig. 2. The expected neutrino
91 energy spectrum at the candidate position is shown in Fig. 3.

92 **2.1 Wagasci module**

93 The dimension of the each Wagasci module is 100cm \times 100cm in the x and y directions
94 and 50cm along the beam direction. Inside the Wagasci module, plastic scintillator bars
95 are aligned as a 3D grid-like structure, shown in Fig. 5, and spaces in the structure are
96 filled with water for the water-in Wagasci module.

97 The total water mass serving as neutrino targets are \sim 0.5 ton. When neutrinos interact
98 with hydrogen, oxygen or carbon, in water and scintillators, charged particles are generated.
99 Neutrino interactions are identified by detecting tracks of charged particles through plastic
100 scintillation bars. Thanks to the 3 D grid-like structure of the scintillator bars, the Wagasci
101 module has 4π angular acceptance for charged particles. Furthermore, adopting a 5cm grid
102 spacing, short tracks originated from protons and charged pions can be reconstructed with
103 high efficiency. Thin plastic scintillator bars (thickness \sim 0.3cm) are used for the Wagasci
104 module to reduce the mass ratio of scintillator bars to water, because neutrino interactions
105 in the scintillator bars are a background for the cross section measurements. Scintillator
106 bars whose dimensions are 2.5cm \times 0.3cm \times 100cm are used for the Wagasci module. The
107 total number of channels in one Wagasci module is 1280.

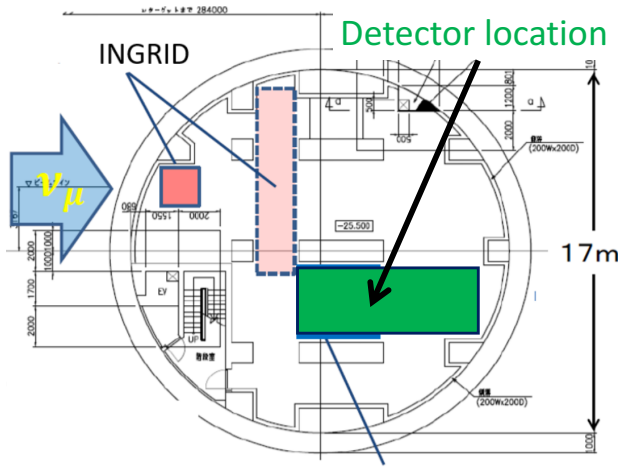


Figure 2: Candidate detector position in the B2 floor of the near detector hall.

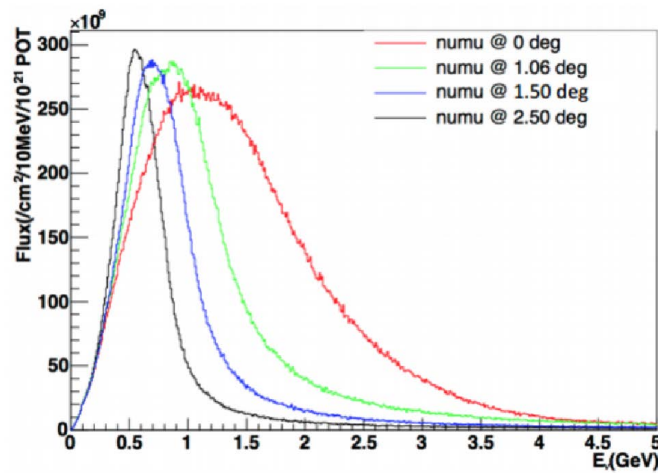


Figure 3: Neutrino energy spectrum at the candidate detector position(red, off-axis 1.5 degree). The spectrum at the ND280 site (black, off-axis 2.5 degree) is also shown.

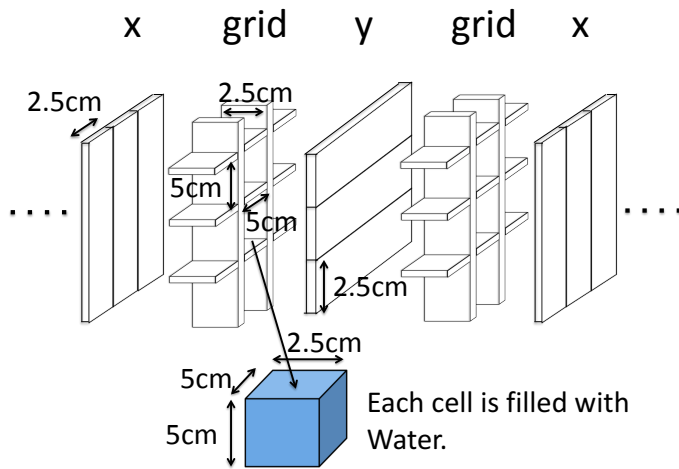


Figure 4: Schematic view of 3D grid-like structure of plastic scintillator bars inside the central detector.

108 2.2 INGRID Proton module

109 INGRID Proton module is a neutrino detectors of the T2K experiment. It is composed only
110 with scintillator bars in its tracking region. (Add more explanation here.) It was installed
111 at the neutrino beam axis on the SS floor of the T2K near detector hall in 2010, and had
112 been used for neutrino cross section measurements. In August 2017, it was moved to the
113 B2 floor of the same detector hall by J-PARC T59 after getting the approval from T2K
114 to use them. J-PARC T59 is performing neutrino beam measurement using the detector
115 from October 2017, and the measurement will continue until May 2018.

116 2.3 Baby MIND

117 The Baby MIND is the downstream Muon Range Detector. It also works as a magnet and
118 provides the charge identification capability as well as magnetic momentum measurement
119 for high energy muons.

120 The Baby MIND collaboration ¹ submitted a proposal to the SPSC at CERN, SPSC-P-
121 353. The project was approved by the CERN research board as Neutrino Platform project
122 NP05 and constructed. The detector consists of 33 magnet modules, each 3500 mm ×
123 2000 mm × 50 mm (30 mm steel) with a mass of approximately 2 tonnes. Of these magnet
124 modules, 18 are instrumented with plastic scintillator modules.

¹Contact person: E. Noah, Spokesperson: A. Blondel, Deputy spokesperson: Y. Kudenko

tmp.pdf

Figure 5: tmp.

125 **2.3.1 Magnet modules**

126 The Baby MIND is built from sheets of iron interleaved with scintillator detector modules
127 but unlike traditional layouts for magnetized iron neutrino detectors (e.g. MINOS) which
128 tend to be monolithic blocks with a unique pitch between consecutive steel segments and
129 large conductor coils threaded around the whole magnet volume, the Baby MIND iron seg-
130 ments are all individually magnetized as shown in Fig. 6, allowing for far greater flexibility
131 in the setting of the pitch between segments, and in the allowable geometries that these
132 detectors can take.

133 The key design outcome is a highly optimized magnetic field map. A double-slit con-
134 figuration for coil winding was adopted to increase the area over which the magnetic flux
135 lines are homogeneous in B_x across the central tracking region. Simulations show the
136 magnet field map to be very uniform over this central tracking region covering an area of
137 $2800 \times 2000 \text{ mm}^2$, Fig. 7. The B_x component dominates in this region, with negligible B_y
138 and B_z . This was confirmed by measuring the field with 9 pick-up coils wound around the
139 first module. Subsequent modules were equipped with one pick-up coil. Test results on
140 the 33 modules show all to achieve the required field of 1.5 T for a current of 140 A, with
141 a total power consumption of 11.5 kW. The polarity of the field map shown in Figure 7
142 (middle) can be reversed by changing the power supply configuration.

143 **2.3.2 Scintillator modules**

144 Each of the 18 scintillator modules is constructed from 2 planes of horizontal counters (95
145 counters in total) and 2 planes of vertical counters (16 counters in total) [?], arranged
146 with an overlap between planes to achieve close to 100% hit efficiency for minimum ioniz-
147 ing muons. The arrangement of planes within a module is vertical-horizontal-horizontal-
148 vertical. This arrangement was the result of an assembly approach whereby each plane

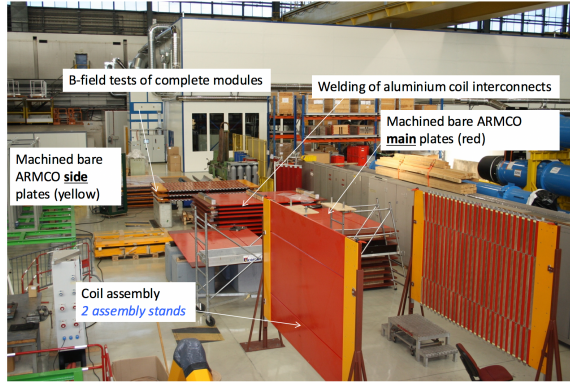


Figure 6: Magnet assembly zone at CERN.

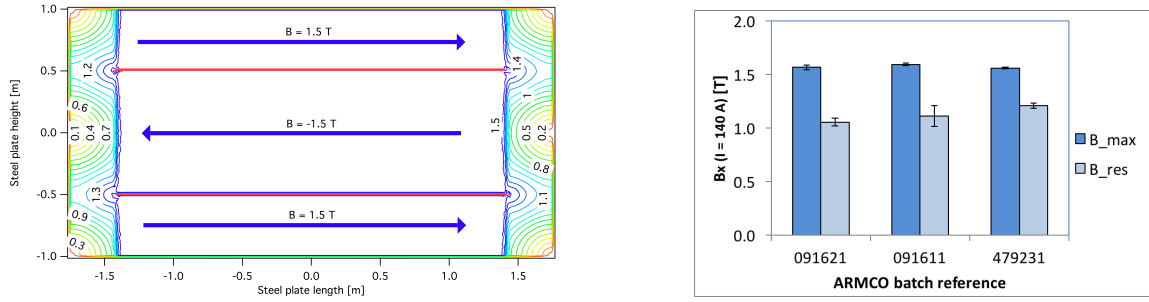


Figure 7: Left) Magnetic field map with a coil along 280 cm of the length of the plate. Right) Measured B field for 33 modules.

149 was built from 2 half-planes, with each half plane consisting of a horizontal plane and a
 150 vertical plane. The scintillator bars are held in place using structural ladders that align
 151 and maintain the counters, Figure 8. No glue is used in the process, so counters can be
 152 replaced. Aluminum sheets front and back provide light tightness.

153 The plastic scintillator counters were made from 220 mm-wide slabs, consisting of
 154 extruded polystyrene doped with 1.5% paraterphenyl (PTP) and 0.01% POPOP. They were
 155 cut to size then covered with a 30-100 μm thick diffuse reflector resulting from etching of
 156 the surface with a chemical agent [?, ?]. The horizontal counter size is $2880 \times 31 \times 7.5 \text{ mm}^3$,
 157 with one groove along the length of the bar in which sits a wavelength shifting fiber from
 158 Kuraray. The vertical counter size is $1950 \times 210 \times 7.5 \text{ mm}^3$, with one U-shaped groove
 159 along the bar. On each counter, two custom connectors house silicon photomultipliers,
 160 MPPC type S12571-025C from Hamamatsu, either side of the horizontal counter, and
 161 both connectors at the top for the vertical counter. This geometrical configuration for
 162 vertical counters was chosen for ease of connectivity to the electronics, and maintenance
 163 operations.



Figure 8: Scintillator modules assembly. Left) top of front half-module showing vertical counters, and the spacers-ladders that set the pitch between horizontal counters and hold them in place. Middle) rear half-module showing horizontal counters on their ladders. Right) Assembled rear half-module, the front half-module can be seen in the background.

164 A total of 1744 horizontal counters and 315 vertical counters (including spares) were
 165 produced at the Uniplast company (Vladimir, Russia).

166 2.3.3 Electronics

167 The Baby MIND electronic readout scheme includes several custom-designed boards [?].
 168 The revised version is shown in Figure 9. At the heart of the system is the electronics
 169 Front End Board (FEB), developed by the University of Geneva. The readout system
 170 includes two ancillary boards, the Backplane, and the Master Clock Board (MCB) whose
 171 development has been managed by INRNE (Bulgarian Academy of Sciences) collaborators.

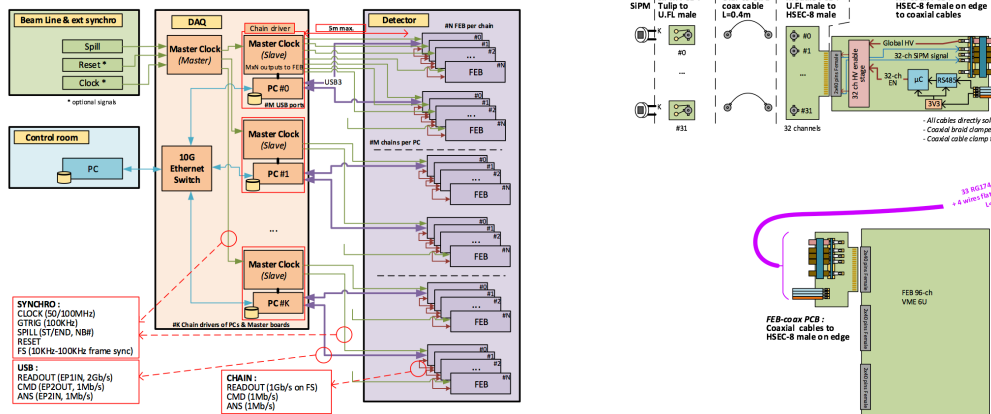


Figure 9: Left) Baby MIND electronics readout scheme. Right) SiPM-to-FEB connectivity.

172 The FEBv2 hosts 3 CITIROC chips that can each read in signals from 32 SiPMs [?].
 173 Each signal input is processed by a high gain, and a separate low gain, signal path. The
 174 outputs from the slow shapers can be sampled using one of two modes: a mode with an

externally applied delay, and a peak detector mode. A faster shaper can be switched to either HG or LG paths, followed by discriminators with adjustable thresholds providing 32 individual trigger outputs and one OR32 trigger output. An Altera ARIA5 FPGA on the FEBv2 samples these trigger outputs at 400 MHz, recording rising and falling times for the individual triggers and assigning time stamps to these. Time-over-threshold from the difference between falling and rising times gives some measure of signal amplitude, used in addition to charge information and useful if there is more than one hit per bar within the deadtime due to the readout of the multiplexed charge output of $\sim 9 \mu\text{s}$. The ARIA5 also manages the digitization of the sampled CITIROC multiplexed HG and LG outputs via a 12-bit 8-ch ADC.

The internal 400 MHz clock on the FEBv2 can be synchronized to a common 100 MHz clock. The synchronization subsystem combines input signals from the beam line into a digital synchronization signal (SYNC) and produces a common detector clock (CLK) which can eventually be synchronised to an external experiment clock. Both SYNC and CLK signals are distributed to the FEBs. Tests show the FEB-to-FEB CLK(SYNC) delay difference to be 50 ps (70 ps). Signals from the beam line at WAGASCI include two separate timing signals, arriving 100 ms and $30 \mu\text{s}$ before the neutrino beam at the near detectors. The spill number is available as a 16-bit signal.

2.4 Side muon range detector

Four Side-MRD modules for tracking secondary particles from neutrino interactions will be constructed by the end of January 2018. Each Side-MRD module is composed of 11 steel plates and 10 layers of total 80 scintillator slabs installed in 13 mm gaps between the 30 mm thick plates. Each steel plate size is $30 \times 1610 \times 1800 \text{ mm}^3$. Total module size is $2236 \times 1630 \times 975 \text{ mm}^3$ as shown in Fig. 10, weight is ~ 8.5 ton.

Scintillator bars were manufactured by Uniplast company in Vladimir, Russia. Polystyrene based scintillators were extruded with thickness of 7 mm, then cut to the size of $7 \times 200 \times 1800 \text{ mm}^3$. Dopant composition is 1.5% PTP and 0.01% POPOP. Scintillator surface was etched by a chemical agent to form a white diffuse layer with excellent reflective performance. Ideal contact between the scintillator and the reflector raises the light yield up to 50% comparing to an uncovered scintillator. Sine like groove was milled along the scintillator to provide uniform light collection over the whole scintillator surface. WLS Y11 Kuraray fiber of 1 mm diameter is glued with an optical cement EJ-500 in the S-shape groove as shown in Fig. 11. Bending radius is fixed to 30 mm that was specified to be safe for Kuraray S-type fibers. Both ends of the fiber are glued into optical connectors (Fig. 12) which mounted within a scintillator body.

The plastic molded connectors provide an interface to SiPMs, Hamamatsu MPPC S13081-050CS(X1) used for the WAGASCI detector. Optical coupler of this type (so-called Baby-mind type of optical connector) consists of two parts (see Fig. 12): an container for the MPPC and a ferrule with the fiber. The ferrule is glued in the scintillator, and its end

214 with glued in WLS fiber was polished. Both parts of the optical coupler are latched by a
 215 snap-like mechanism: a locking groove inside the container and matching ring protuber-
 216 ance on the ferrule. To ensure the optical contact a foam spring made of sponge rubber
 217 presses the MPPC to the fiber end (Fig. 13).

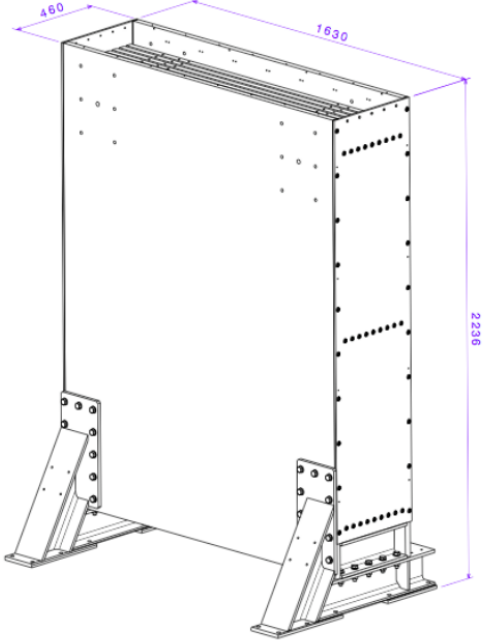


Figure 10: Support structure of the Side-MRD module.

218 Scintillators for the Side-MRD modules had been assembled at INR in Russia, and
 219 shipped to Japan in July 2017. The light yield for each scintillator was measured with
 220 cosmic rays at INR and at YNU in Japan after delivery. Parameters measured at the
 221 center of the counter were : the light yields LY_1 and LY_2 at both ends, the light yield
 222 asymmetry between the ends calculated as $100\% \times \frac{LY_1 - LY_2}{LY_1 + LY_2}$. After tests at INR we selected
 223 324 counters from measured 332 ones with the mean light yield of 45 p.e./MIP ($LY_1 + LY_2$)
 224) and the asymmetry value less than 10 %. The measuremens at YNU yielded the average
 225 total light yield of about 40 p.e./MIP which varies in range from 32 to 50 p.e./MIP (Fig.
 226 14 (left)). Only two counters showed relatively high asymmetry close to 25 % as shown in
 227 Fig. 14 (right). Using the results of the quality assurance test we selected 320 scintillator
 228 counters for the Side-MRD modules.

229 We also measured the time resolution for a combination of four counters piled each on
 230 another one. Time resolution for a single counter is determined as rms of $(T_{left} - T_{right})/2$
 231 distribution. The difference of times was chosen to remove the correlated time fluctuation

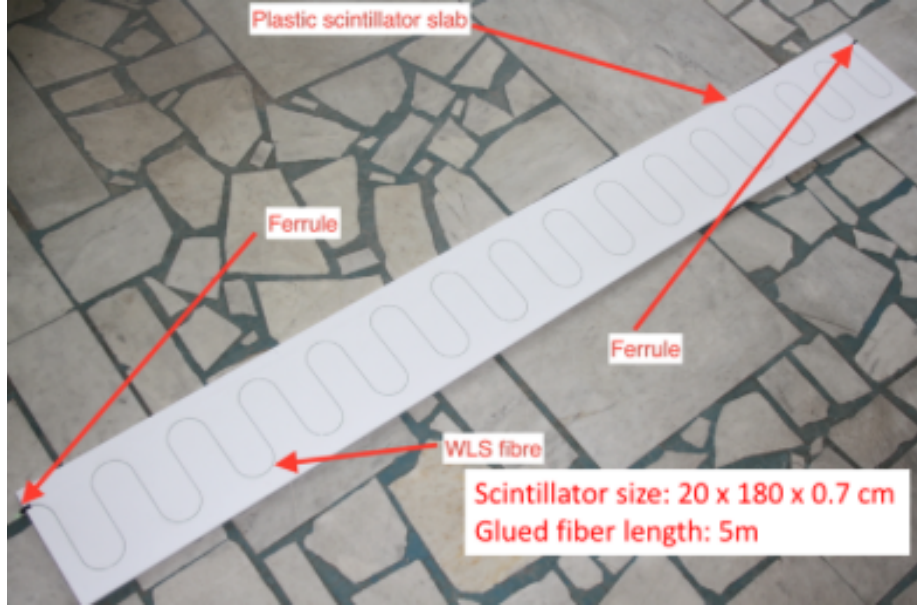


Figure 11: Scintillator bar of the Side-MRD modules.

caused by a start trigger signal. The average result for four counters is $\sigma_T = 1.04$ ns (Upper left plot in Fig. 15). For a set of n counters the time resolution is calculated as $\frac{(T_L-T_R)_1+(T_L-T_R)_2+\dots+(T_L-T_R)_n}{2 \times n}$. The result of combination of 2, 3, 4 counters is 0.79 ns, 0.66 ns and 0.58 ns, correspondently (Fig. 15).

Construction of Side-MRD modules will be done from November 2017 to January 2018 at Yokohama National University, then they will be transported to J-PARC and will be installed at B2 floor of the T2K near detector hall before T2K beam in March 2018.

3 Physics goals

We will measure the differential cross section for the charged current interaction on H₂O and Hydrocarbon(CH)). The water-scintillator mass ratio of the Wagasci module is as high as 5:1 and the high purity measurement of the cross section on H₂O is possible. One experimental option is to remove water from one of the two Wagasci modules. The water-out WAGASCI module will allow to measure pure-CH target interactions with very low momentum-threshold for protons. It will also benefit to subtract the background from interaction with scintillator in the water target measurement. Another option is to add

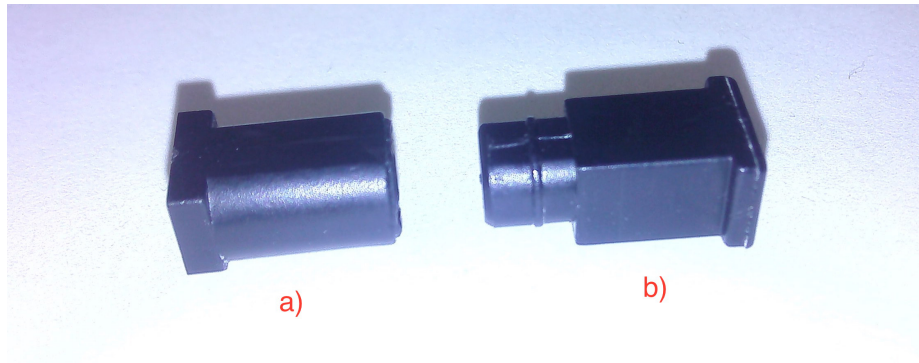


Figure 12: Optical connector for the Side-MRD scintillator. a) MPPC cover. b) Ferrule.

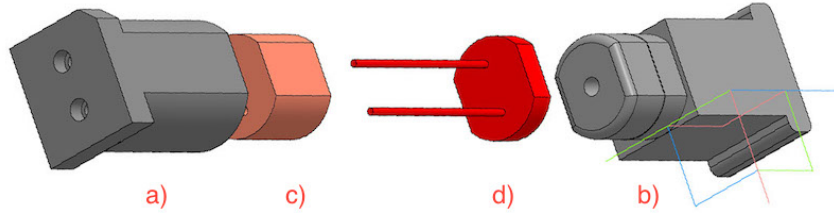


Figure 13: Scheme of the MPPC placement in optical connector. a) MPPC cover. b) Ferrule. c) Spring (sponge rubber). d) MPPC.

247 the T2K proton module which is fully made of plastic scintillators. It will allow the high
 248 statistics comparison of cross section between H₂O and CH and also comparison with
 249 the ND280 measurement. The actual configuration will be optimized with detailed MC
 250 simulation by 2018 Summer.

251 Our setup allows the measurements of inclusive and also exclusive channels such as 1- μ ,
 252 1- μ 1p, 1- μ 1 $\pi\pm np$ samples, former two of which are mainly caused by the quasi-elastic and
 253 2p2h interaction and the latter is mainly caused by resonant or coherent pion production
 254 and deep elastic scattering. In general, an accelerator produced neutrino beam spectrum
 255 is wide and the energy reconstruction somehow rely on the neutrino interaction model.
 256 Therefore, recent neutrino cross section measurement results including those from T2K
 257 are given as a flux-integrated cross section rather than cross sections as a function of
 258 the neutrino energy to avoid the model dependency. We can provide the flux-averaged
 259 cross section. In addition, by combining our measurements with those at ND280, model-
 260 independent extraction of the cross section for narrow energy region becomes possible.

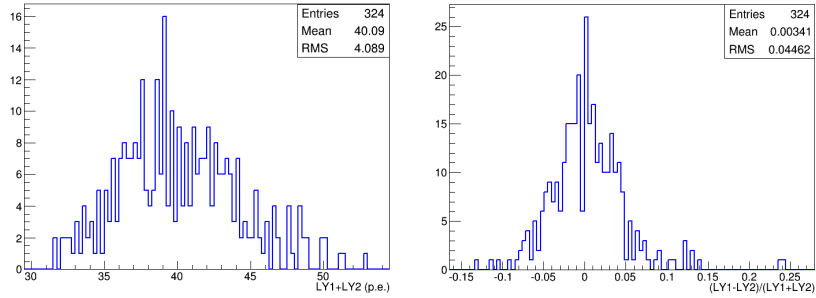


Figure 14: Total light yield distribution (left) and light yield assymetry (right) measured at YNU.

261 This method was demonstrated in [?] and also proposed by P** (NUPRISM).

262 3.1 Expected number of events

263 Expected number of neutrino events after the event selections is evaluated with Monte
 264 Carlo simulations as we will discuss in Section 6. 2.41×10^4 CC events are expected in
 265 two WAGASCI modules after the selection with 1×10^{20} POT in neutrino-mode, and its
 266 purity is 75.5 %. In case we choose the option with one WAGASCI module and the T2K
 267 proton module, 1.2×10^4 CC events are expected in the WAGASCI module and $\sim 1 \times 10^4$
 268 CC events are expected in the T2K proton module. In case we choose the option with one
 269 water-in WAGASCI module and one water-out WAGASCI module, 1.2×10^4 CC events are
 270 expected in the water-in module and 0.24×10^4 CC events are expected in the water-out
 271 module.

272 3.2 Pseudo-monochromatic beam by using different off-axis fluxes

273 The off-axis method gives narrower neutrino spectrum, and the peak energy is lower for
 274 larger off-axis angle. There still remains high energy tail mainly due to neutrinos from
 275 Kaon decay. The off-axis angle of the Wagasci location is 1.5 degree and different from the
 276 ND280 2.5 degree. Top two plots of Fig. 16 show the energy spectra of fluxes and neutrino
 277 interaction events at these two different location. The high energy tail of ND280 flux can
 278 be somehow subtraction by using the Wagasci measurement. The low energy part of the
 279 Wagasci flux can be also subtracted by using the ND280 measurement. Bottom two plots
 280 of Fig. 16 demonstrate this method. We can effectively get two fluxes, from 0.2 GeV to
 281 0.9 GeV and 0.6 GeV and 2 GeV and measure flux-integrated cross section for these two
 282 fluxes.

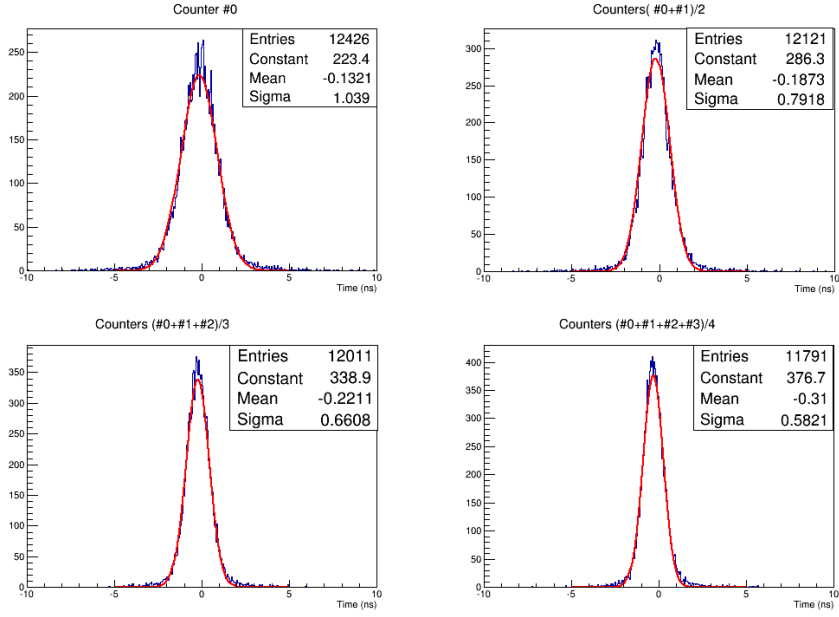


Figure 15: Time resolution for one (upper left) and a set of 2,3,4 Side-MRD counters.

283 3.3 Subjects Wagasci can contribute

284 In T2K experiment, neutrinos interact with bound nucleons in relatively heavy nuclei
 285 (Carbon and Oxygen), so the cross-section is largely affected by nuclear effects. The nuclear
 286 effects are categorized as nucleons' momentum distribution in nucleus, interactions with
 287 correlated pairs of nucleons in nucleus (two particles-two holes, 2p2h), collective nuclear
 288 effects calculated with Random Phase Approximation (RPA) and final state interactions
 289 (FSI) of secondary particles in the nuclei after the initial neutrino interactions.

290 The 2p2h interactions mainly happen through Δ resonance interactions following a
 291 pion-less decay and interactions with a correlated nucleon pair. The 2p2h interactions are
 292 observed in electron scattering experiments (add ref. here) where the 2p2h events observed
 293 in the gap between Quasi-Elastic region and Pion-production region as shown in Fig. ??.
 294 Neutrino experiments also attempt to measure the 2p2h interactions, but separation of the
 295 QE peak and the 2p2h peak is more difficult because transferred momentum (p) and energy
 296 (w) are largely affected by neutrino energies which cannot be determined event-by-event in
 297 the wide energy spectrum of the accelerator neutrino beam. Our model-independent narrow
 298 neutrino spectra extracted from combined analyses of our data and ND280 data are ideal
 299 for searching the 2p2h interaction because clearer separation of the QE peak and the 2p2h
 300 peak is expected. Another way to observe the 2p2h interaction is direct measurement of
 301 proton tracks in CC0 π sample with low detection threshold and full acceptance. Fig. ??

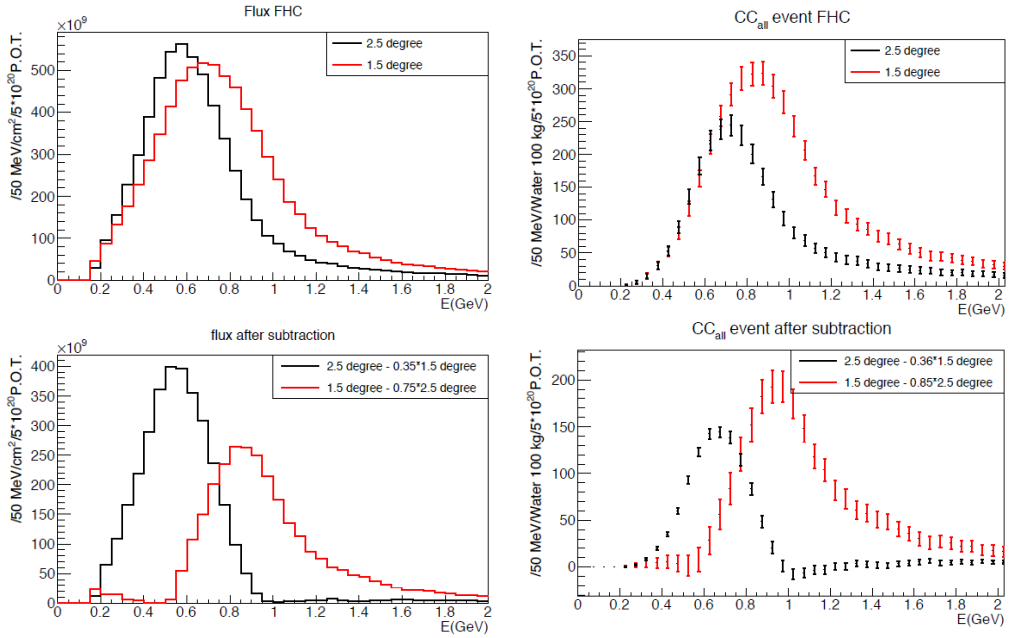


Figure 16: Energy spectra obtained by using different off-axis angle fluxes. Top two plots show the fluxes(left) and spectra of interaction events (right) for ND280 (off-axis 2.5 degree) and Wagasci (off-axis 1.5 degree). Bottom two plots show the fluxes (left) and spectra of interaction events (right) obtained by subtraction of fluxes at ND280 and Wagasci. The error bar is for the statistical error and those in the bottom right plot is obtained assuming the statistical error for ND280 measurement is much smaller than that of Wagasci experiment.

302 shows proton multiplicities in CCQE events and 2p2h events, and Fig. ?? shows opening
 303 angles among two proton tracks in the same samples. The water-out WAGASCI can provide
 304 good sample for the 2p2h interaction search because its low density medium enables the
 305 detection of low momentum protons in addition to the full acceptance.

306 The corrections from collective nuclear effects calculated by RPA as a function of Q^2 are
 307 shown in Fig. ???. The Q^2 dependence of the correction can be tested by measuring angular
 308 distribution of muons in CC1- μ and CC1- $\mu 1p$ events. The uncertainties of the corrections
 309 in low (high) Q^2 regions can be constrained by observing the events with a forward-going
 310 (high-angle) muon, so it is essential to measure muon tracks with full acceptance.

311 T2K experiment is starting to use ν_e CC1 π events for its CP violation search to increase
 312 the statistics. One of the biggest uncertainty of the CC1 π sample comes from the final
 313 state interactions of pions in the nuclei after the initial neutrino interactions because they
 314 change the multiplicity, charge and kinematics of the pions. The multi-pion production

315 events can be migrated into the CC1 π sample due to the FSIs, and they become important
316 backgrounds. We can constrain the uncertainties from the pion FSIs by measuring pion
317 rescattering in the detector and pion multiplicity in ν_μ CCn π sample with low detection
318 threshold and full acceptance for pion tracks. The water-out WAGASCI can provide good
319 sample for the pion FSI studies because its low density medium enables the detection of
320 low momentum pions in addition to the full acceptance.

321 4 Status of J-PARC T59 experiment

322 We had submitted a proposal of a test experiment to test a new detector with a water
323 target, WAGASCI, at the T2K near detector hall to J-PARC PAC on April 2014, and the
324 proposal was approved as J-PARC T59. There are several updates on the project after
325 three years from then. Fist, the start time of neutrino beam measurement is changed from
326 December 2015 to October 2017, and the requested neutrino beam is changed from 1×10^{21}
327 POT of ν beam to 0.8×10^{21} POT of anti- ν beam. Second, the detector configuration is
328 changed. In the original proposal, central neutrino detector are expected to be surrounded
329 by newly developed muon-range detectors (MRDs), but we will use spare neutrino detectors
330 of the T2K experiment instead of them during neutrino beam measurement from October
331 to December 2017. Construction of the newly developed MRDs, Baby-MIND and Side-
332 MRD, is in progress, and they will be installed to the both sides and the downstream of
333 the central neutrino detector from January to March 2018. Then, we will resume neutrino
334 beam measurements from March 2018 and will take the neutrino beam data until May
335 2018.

336 4.1 On-axis beam measurement with Prototype detector

337 Add INGRID water module measurement here.

338 4.2 Plans from October 2017 to May 2018

339 J-PARC MR will extract its proton beam to T2K neutrino beam-line from October to
340 December 2017, and, from March to May 2018. T2K experiment will produce anti-neutrino
341 beam and will accumulate $\sim 8 \times 10^{20}$ POT data during the above period.

342 J-PARC T59 will perform neutrino beam measurements on the B2 floor of the T2K
343 near neutrino detector hall during the above period to test basic performances of the
344 WAGASCI detector and new electronics. During the beam measurements from October to
345 December 2017, one WAGASCI module will be placed between spare neutrino detectors of
346 the T2K experiment, INGRID Proton module and INGRID standard module. Here, the
347 INGRID Proton module is used as a charged particle VETO detector and, the INGRID
348 standard module is used as a downstream muon detector. We had submitted a proposal

349 to use these spare neutrino detectors for the T59 neutrino beam measurements to the T2K
350 collaboration, and we got an approval from T2K.

351 During the beam measurements from March to May 2018, Baby-MIND and two side
352 muon-range detector (Side-MRD) modules will be installed on the downstream and the
353 both sides of the WAGASCI detector, as shown in Fig. 17, to increase angular acceptance
354 for secondary charged particles from neutrino interactions. Add Baby-MIND commission-
355 ing items here!!!

tmp.pdf

Figure 17: J-PARC T59 detector configuration with Baby-MIND and two Side-MRD modules from Mar. to May 2018. (Need to prepare the figure.)

356 Expected number of neutrino events in the WAGASCI detector during the above beam
357 period is evaluated with Monte Carlo simulations. Neutrino beam flux at the detector
358 location is simulated by T2K neutrino flux generator, JNUBEAM, neutrino interactions
359 with target materials are simulated by a neutrino interaction simulator, NEUT, detector
360 responses are simulated using GEANT4-based simulation. The neutrino flux at the detector
361 location, 1.5 degrees away from the J-PARC neutrino beam axis, is shown in Figure 3, and
362 its mean neutrino energy is around 0.68 GeV. An event display of the GEANT4-based
363 detector simulation is shown in Figure 20.

364 To perform the detector performance test, the following event selections are applied to
365 the data. First, track reconstructions are performed in the WAGASCI detector, and the
366 reconstructed vertex is required to be inside a defined fiducial volume, $80 \times 80 \times 32 \text{ cm}^3$
367 region at the center of the detector, to reduce contamination from external backgrounds.
368 Second, at least one charged particle is required to reach to INGRID standard module
369 or Side-MRD modules, and it makes more than two hits in these sub-detectors. With the

370 event selection, expected numbers of the neutrino-candidate events during the beam period
371 are summarized in Table 1. Using the data, we will test the detector performance with
372 $\sim 3\%$ statistical uncertainties.

373 5 Detector performance

374 5.1 Wagasci module

375 To demonstrate the performance of the Wagasci module and also to study the neutrino
376 interaction, the first Wagasci module was installed at the on-axis position, in front of
377 the T2K INGRID horizontal center module in 2016. The INGRID module is made of iron
378 plates and segmented plastic scintillator bars. It's cross sectional size viewed from the beam
379 direction is $1 \text{ m} \times 1 \text{ m}$. The charged current interactions in the Wagasci module are selected
380 by requiring a muon track candidate in the INGRIRD modules. Here, we describe the
381 performance of the Wagasci module evaluated at this T2K on-axis measurement. Figure 18
382 shows the light yeild of channels for muons produced by the interaction of neutrinos in the
383 hall wall. The light yield is sufficiently hgih to get good hit efficieincy. A track search

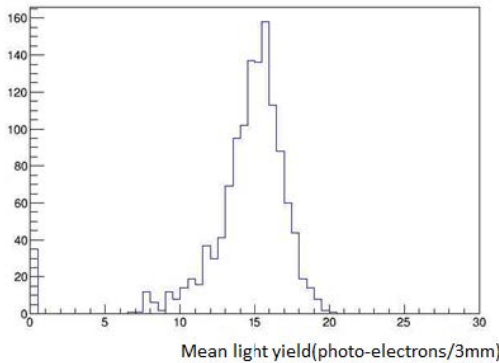


Figure 18: Light yield of channels for muons produced by the interaction of neutrinos in the hall wall.

383 algorithm based on the cellular automaton has been developed using the software tools by
384 the T2K INGRID. The tracking efficiency in 2-dimentional projected plane was evalualted
385 by comparing the reconstructed track in the Wagasci module and the INGRID module and
386 shown in Fig.19. Note that that the tracking efficinency for high angle ($> 70 \text{ deg}$) is not
387 evaluated because of the acceptance of the INGRID module, not because of the limitation
388 of the Wagasci module.
389

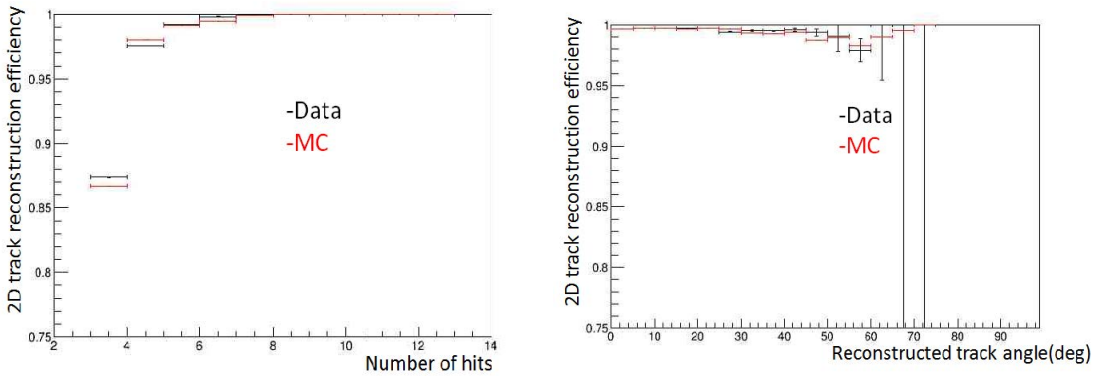


Figure 19: 2D track reconstruction efficiency as a function of number of hits (left) and track angle (right). Here the track angle is the one reconstructed by the INGRID module.

390 5.2 Baby MIND

391 The Baby MIND construction was completed in June 2017, and it was then tested in
 392 June and July 2017 at the Proton Synchrotron experimental hall at CERN with a mixed
 393 particle beam comprising mostly muons whose momenta could be selected between 0.5 and
 394 5 GeV/c. An event display from the summer 2017 tests is shown in Figure 22.

395 All counters were measured at INR Moscow with a cosmic ray setup using the same
 396 type S12571-025C MPPCs and CAEN DT5742 digitizer [?]. The average light yield (sum
 397 from both ends) was measured to be 37.5 photo-electrons (p.e.) per minimum ionizing
 398 particle (MIP) and 65 p.e./MIP for vertical and horizontal counters, respectively. After
 399 shipment to CERN, all counters were tested once more individually with an LED test setup
 400 [?]. 0.1% of counters failed the LED tests and were therefore not used during the assembly
 401 of modules.

402 5.3 Side muon range detector

403 6 MC studies

404 6.1 Detector simulation

405 Expected number of neutrino events in the WAGASCI detector is evaluated with Monte
 406 Carlo simulations. Neutrino beam flux at the detector location is simulated by T2K neutrino
 407 flux generator, JNUBEAM, neutrino interactions with target materials are simu-
 408 lated by a neutrino interaction simulator, NEUT, detector responses are simulated using
 409 GEANT4-based simulation. The neutrino flux at the detector location, 1.5 degrees away

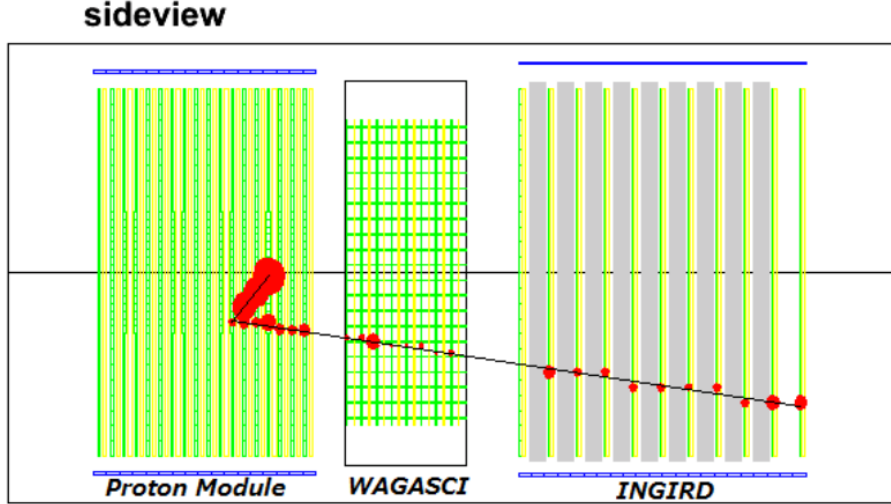


Figure 20: J-PARC T59 event display of a neutrino event in the GENAT4-based detector simulation.

from the J-PARC neutrino beam axis, is shown in Figure 3, and its mean neutrino energy is around 0.68 GeV.

6.1.1 Detector geometry

The detector geometry in the GEANT4-based simulation is slightly different from the actual detector as shown in Fig. 24. The active neutrino target region consists of four WAGASCI modules, and each WAGASCI detector has the dimension with $100\text{ cm} \times 100\text{ cm}$ in the x and y directions and 50 cm along the beam direction. An event display of a MC event in the WAGASCI detectors is shown in Figure ???. Two Side-MRD modules are installed at both sides of the WAGASCI modules, and each Side-MRD module consists of ten iron plates whose dimension is 3 cm (thickness) \times 180 cm (height) \times 320 cm (width). The distance between the Side-MRD modules and WAGASCI modules is 60 cm. The downstream-MRD equivalent to the Baby-MIND is installed at the downstream of the WAGASCI modules. The downstream-MRD consists of ten iron plates whose dimension is 3 cm (thickness) \times 180 cm (height) \times 320 cm (width) and another ten iron plates whose dimension is 6 cm (thickness) \times 180 cm (height) \times 320 cm (width). The distance between

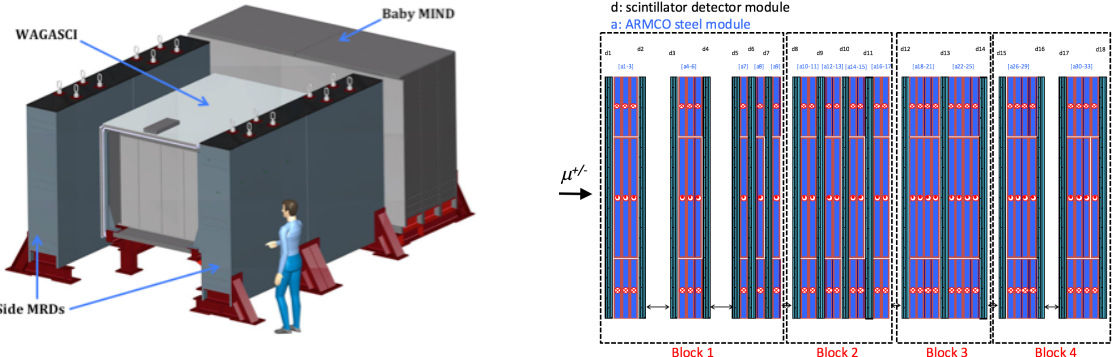


Figure 21: Left) WAGASCI modules: flanked by 2 side muon range detectors (sMRD) and one downstream muon detector (Baby MIND). Right) side view layout of the Baby MIND during beam tests at CERN.

425 the downstream-MRD modules and WAGASCI modules is 60 cm.

426 In order to estimate backgrounds from neutrino interactions in the wall and floor of the
427 experimental hall, the geometry of the experimental hall is implemented in the GEANT4-
428 based detector simulation.

429 **6.1.2 Response of detector components**

430 The energy deposit inside the scintillator is converted into the number of photons. The
431 effects of collection and attenuation of the light in the scintillator and the WLS fiber are
432 simulated, and the MPPC response is also taken into account. The light yield is smeared
433 according to statistical fluctuations and electrical noise.

434 **6.2 Track reconstruction**

435 To select neutrino interaction from the hit patterns, a track reconstruction algorithm is
436 developed. The flow of the track reconstruction is as follows.

- 437 1. Two-dimensional track reconstruction in each sub-detectors
- 438 2. Track matching among the sub-detectors
- 439 3. Three -dimensional track reconstruction

440 Add explanation about two-dim reco, track matching and three-dim reco here.

441 **6.3 Event selection**

442 First, the events with the track which starts in 5 cm from the wall of the WAGASCI module
443 are rejected to remove the background from the outside.

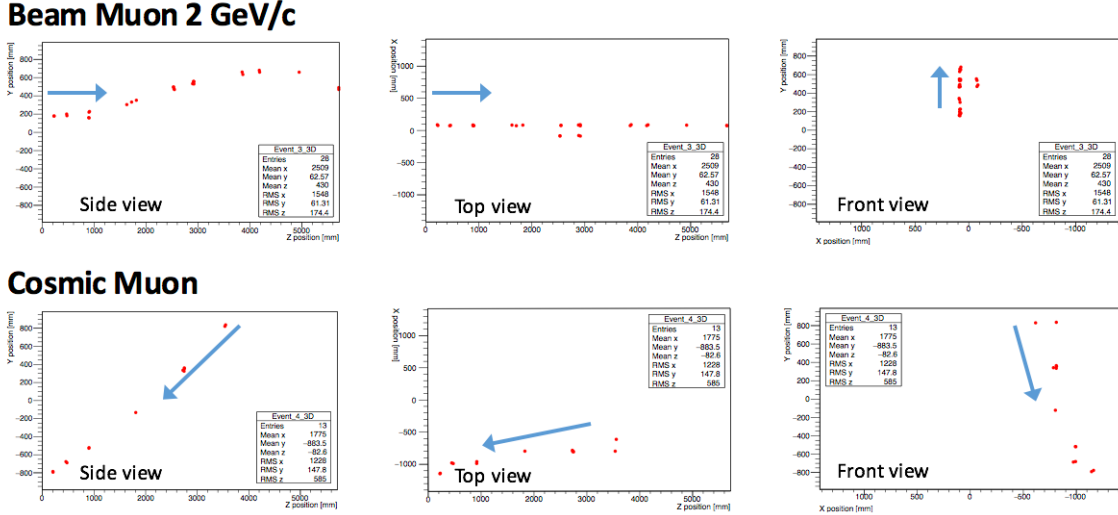


Figure 22: Comparison of a beam muon and cosmic muon in the three different geometrical projections of the detector. The beam impinges on the detector from the left. The arrows indicate the direction of travel of these muons. The direction of the cosmic muon is inferred from timing information.

Second, to reject backgrounds from NC and neutral particles, the longest tracks are required to penetrate more than one (five) iron plates in Side-MRD modules (Baby-MIND). Then, in order to measure muon momentum, the longest tracks are required to stop in MRDs (Side-MRD modules and Baby-MIND) or penetrate all iron plates.

Table 1 and 2 show numbers of the selected events after each event election in neutrino-mode and antineutrino-mode respectively. As for the neutrino-mode, 2.12×10^4 CC events are expected with 1×10^{21} POT, and the purity is 81.3 %. The main background for the neutrino-mode is the neutrino interactions in the scintillators inside the WAGASCI detector. As for the antineutrino-mode, 0.83×10^4 CC events are expected with 1×10^{21} POT, and the purity is 62.0 %. The main background for the antineutrino-mode is the wrong sign contamination from ν_μ events and the antineutrino interactions in the scintillators inside the WAGASCI detector.

Figure 25 and 26 show the reconstructed angles of the longest tracks in the selected events in the neutrino-mode and the anti-neutrino mode respectively.

Figure 27 and 28 show the iron plane numbers corresponding to the end points of the longest tracks in the selected events.

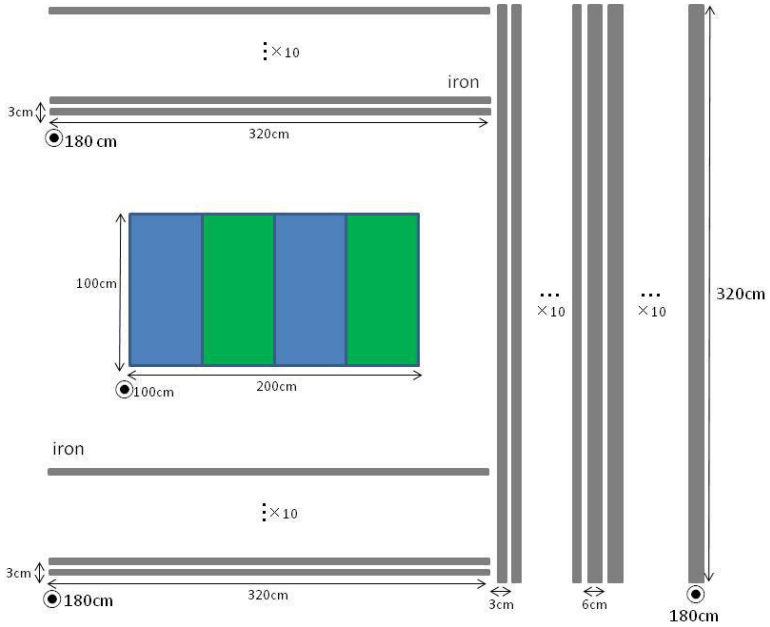


Figure 23: Geometry of the detectors in the Monte Carlo simulation.

460 6.4 Cross section measurements on water

461 In the water target events, the background from interaction with scintillators has to be
 462 subtracted by using the measurement of the hydrocarbon target.

463 6.4.1 Charged current cross section measurement

464 7 Standalone WAGASCI-module performances

465 In the previous sections, the WAGASCI detector was studied using the Muon Range De-
 466 tectors. In this section, the standalone abilities of WAGASCI module are presented. Using
 467 the WAGASCI configuration presented in Section 6, we have evaluated that only 7% of
 468 the muons will be stopped in one of the WAGASCI modules. THowerver, this proportion
 469 increases to 53% for pions and 73% for protons produced by neutrino interactions at 1.5°
 470 off-axis. Figure 29 shows the momentum distribution of these daughter particles as well as
 471 for the sub-sample stopped in one of the WAGASCI modules. Therefore, the study of the
 472 standalone abilities of the WAGASCI module in this section are dominantly motivated by:

- 473 • the accurate measurement of the neutrino interaction final states. Though most of the

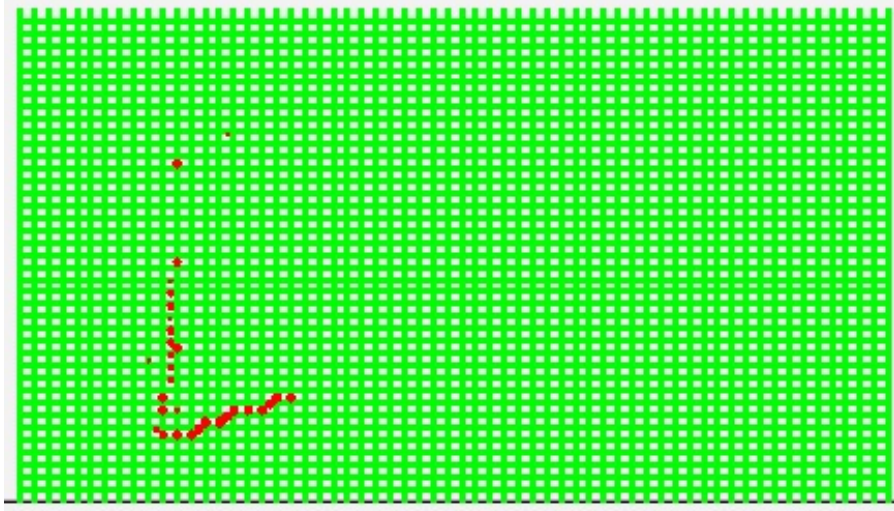


Figure 24: An event display of MC event in WAGASCI detectors. Green lines are scintillators and red circles are the hit channels.

474 muons will be reconstructed and identified in the MRDs, the hadronic particles will
 475 predominantly stops in one WAGASCI module. One has therefore to rely exclusively
 476 on the WAGASCI module information alone to reconstruct, identify and measure the
 477 momentum of pions or protons.

- 478 • the coverage of the MRDs is not 4π . Using the WAGASCI module information can
 479 therefore help to constraint the particles that exits the WAGASCI module but do
 480 not geometrically enters any MRD.
- 481 • the particle identification of low momenta muons $p_\mu < 300 \text{ MeV}/c$ that will leave only
 482 few hits in the MRD. Using the WAGASCI module information will clearly enhance

Table 1: Expected number of the neutrino-candidate events in two WAGASCI modules after the event selections with 1×10^{21} POT in neutrino-mode.

Cut	CC	NC	Scinti Bkg.	Total
Reconstructed	45233	1749.27	9396.46	56378.8
FV	37876.8	1471.02	7869.57	47217.4
Pene. iron	28160.7	593.267	5750.79	34504.7
Stop/Penetrate MRDs	21195.4	534.914	4346.06	26076.4
after all cuts	81.3 %	2.1 %	16.7 %	100 %

Table 2: Expected number of the antineutrino-candidate events in two WAGASCI modules after the event selections with 1×10^{21} POT in antineutrino-mode.

Cut	CC	NC	Scinti Bkg.	Wrong sign bkg	Total
Reconstructed	16249.1	268.082	4468.83	5826.95	26813.0
FV	13644.7	223.211	3746.85	4866.36	22481.0
Pene. iron	10430.8	76.9422	2881.81	3901.35	17290.9
Stop/Penetrate MRDs	8328.73	71.2382	2240.59	2802.98	13443.5
after all cuts	62.0 %	0.5 %	16.7 %	20.9 %	100 %

483 the particle identification.

484 This study is based on an original study done for the ND280 upgrade target, with some
 485 modifications. Though the cell size is similar to the WAGASCI configuration presented
 486 in Section 6, the external dimensions are different ($186.4 \times 60 \times 130$ cm 3). Whenever the
 487 results are presented with this external size and this parameter is likely to impact the
 488 result, it will be mentioned.

489 Note that in this section, a simplified reconstruction algorithm presented in Section 7.1 is
 490 used. The fiducial volume is chosen accordingly as the inner cube of the module which
 491 surfaces are distant of $4 \times$ scintillator space = 10 cm from the module external surfaces.
 492 The neutrino interactions are simulated using NEUT v5.3.2. The NEUT input neutrino
 493 flux is estimated using JnuBeam v13a and assuming the detector to be located at 1.5°
 494 off-axis, as in Section 6. Note that the event reconstruction efficiency as a function of true
 495 neutrino energy might be changed at 1.5° , due for example to different Q^2 distributions. For
 496 this reason, one has to note that the reconstruction results might slightly be changed from
 497 2.5° and 1.5° . To avoid a similar change on the particle-only reconstruction efficiencies,
 498 they will be presented as a function of variables that completely characterize the particle
 499 kinematic state, *i.e.* its momentum and angle. Figure 30 shows the vertices distributions
 500 of the daughter particles of neutrinos interacting one standard WAGASCI water-module.
 501 In this section, we will show the detector reconstruction and particle identification in this
 502 phase space, both for leptonic and hadronic particles. We will finally show an empty
 503 WAGASCI module can highly enhance the ability to constrain the neutrino interaction
 504 final state which is critical to reduce the corresponding uncertainties.

505 **7.1 Reconstruction algorithm**

506 **7.1.1 Description**

507 For this section, an ideal “simulated” reconstruction is developed. A particle is recon-
 508 structed if:

- 509 1. The particle is charged.

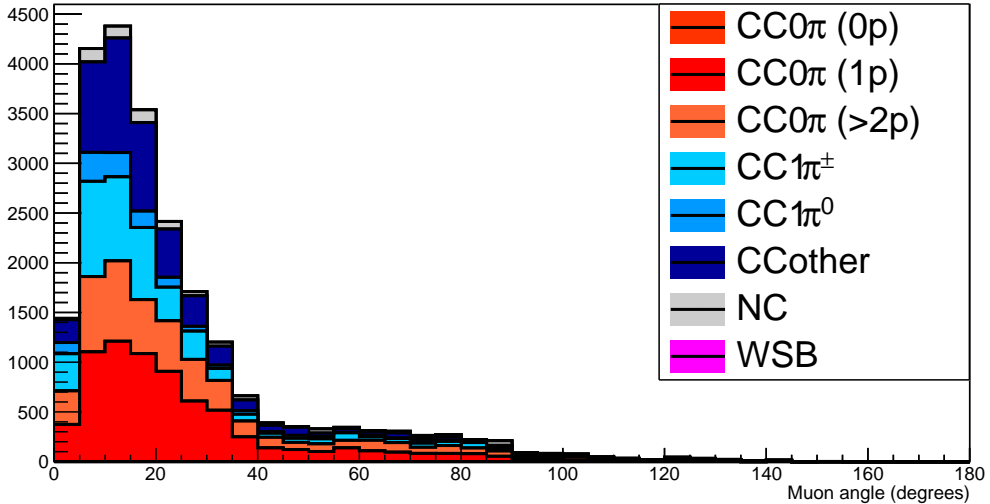


Figure 25: The reconstructed angles of the longest tracks in the selected events in the neutrino-mode.

- 510 2. Lets at least one hit (energy deposit > 2.5 photo-electron) in a scintillator.
 511
 512 3. The particle enters one TPC and let one hit in the tracker.
 513 Or
 514
 515 • The particle should be long enough to be reconstructed by the detector in at
 516 least 2 out of 3 views (XZ, YZ, XY). The length criterion requires the particle
 517 to let at least 4 hits in the detector. In the “less favourable case” of pure
 518 longitudinal or transverse going tracks, it represents a the track length of $L_{track} \geq$
 519 $4 \times$ scintillator space = 10.0 cm.
 520 • In the views where particles pass the length criterion, the particle shall not
 521 be superimposed with longer tracks in at least two views. The superposition
 522 criterion is estimated with the distance inter-tracks (DIT) which corresponds to
 523 the orthogonal distance between two tracks at the ending point of the shortest
 524 one (see Figure 31). For a track 1, the superposition criterion is tested with
 525 every longer tracks that starts at the same vertex. Let \vec{p}_1^i the vector of track
 526 1, and p_1^a its projections in the XZ, YZ and XY planes respectively for $i=1,2,3$.

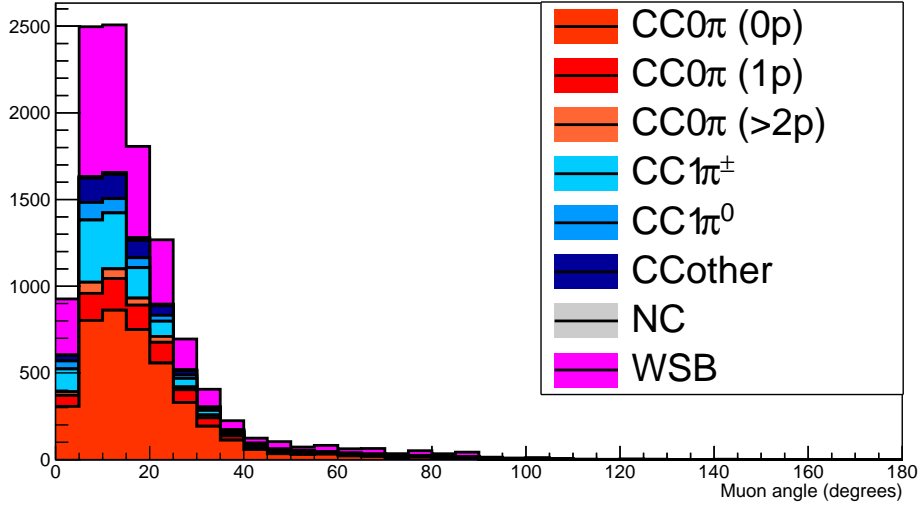


Figure 26: The reconstructed angles of the longest tracks in the selected events in the antineutrino-mode.

527 Note that these are projections in a 2D planes and not on a direction vector. In
 528 this case, the relative angle between the track 1 and a longer track 2 (of vector
 529 \vec{p}_2) in a view a is given by:

$$\cos \theta = \frac{\vec{p}_1^a \cdot \vec{p}_2^a}{\|\vec{p}_1^a\| \|\vec{p}_2^a\|} \quad (1)$$

530 and the distance inter track is given by:

$$DIT = \|\vec{p}_1^a\| \sin \theta \quad (2)$$

531 The DIT should be higher than $4 \times$ scintillator width for the track 1 to be not
 532 superimposed with the track 2 in the view a, which also corresponds to 10.0 cm
 533 in the nominal configuration.

534 7.1.2 Performances

535 The particle-only reconstruction efficiencies and the reconstruction threshold in momenta
 536 are shown in Table 3. This threshold is defined as the maximal momentum for which the
 537 reconstruction efficiency is smaller than 30%. The thresholds in muon and pion momenta

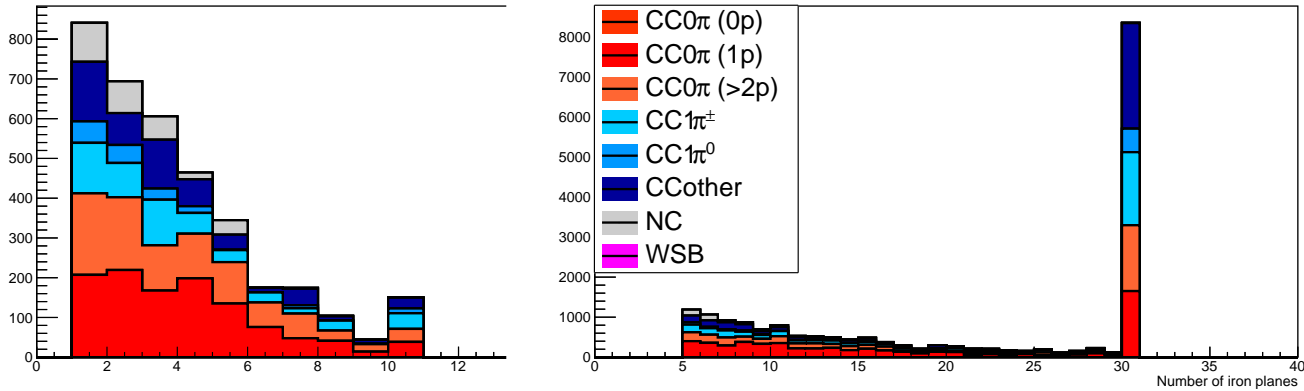


Figure 27: Iron plane numbers in Side-MRD (left) and Baby-MIND (right) corresponding to the end points of the longest tracks in the selected events in the neutrino-mode.

	μ	π	p
Reconstruction Efficiency	79%	52%	26%
Momentum threshold	150 MeV/c	150 MeV/c	550 MeV/c

Table 3: Reconstruction efficiency and momentum threshold for muons, pions and protons. The threshold is defined as the maximal momentum for which particles have a reconstruction efficiency smaller than 30%.

538 are 150 MeV/c. Most of the muons are above this threshold (see Figure 30) which leads
539 to a 79% reconstruction efficiency.

540 The lower pion and proton efficiencies (respectively 52% and 26%) are due to lower
541 efficiencies for similar momenta than muons, coming from strong interactions as shown
542 on Figures 32. Efficiencies of each particle type tend to decrease in the backward region
543 due to particle lower momenta. However, for a fixed momentum value, the reconstruc-
544 tion efficiency is almost uniform which confirms the ability of the WAGASCI detector to
545 reconstruct high angle tracks.

546 The reconstruction is thereafter tested on neutrino events. Table 4 summarizes the
547 number of reconstructed events and efficiencies for each interaction type. As expected
548 from the high muon reconstruction efficiency, the charged current interactions have recon-
549 struction efficiencies $\geq 85\%$.

550 The reconstruction efficiencies as a function of the neutrino energy and muon kinematics
551 are respectively shown on Figure 33 and 34.

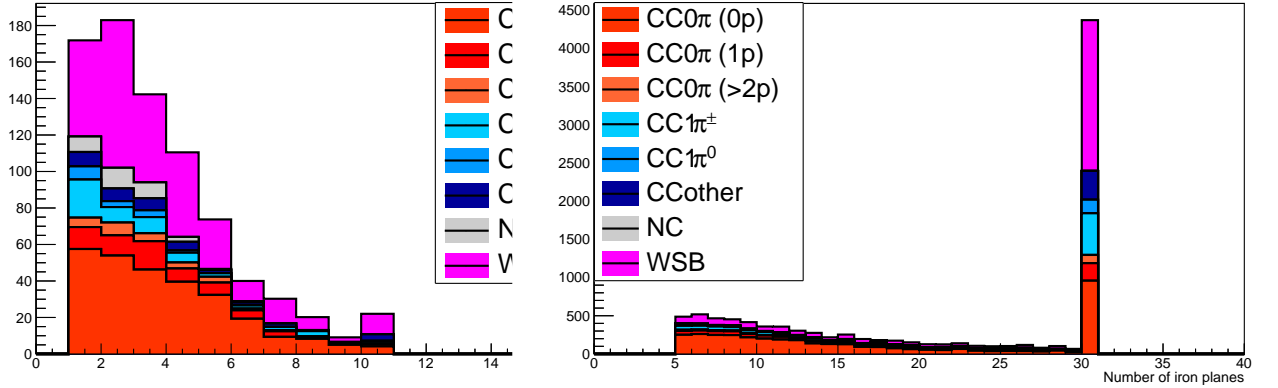


Figure 28: Iron plane numbers in Side-MRD (left) and Baby-MIND (right) corresponding to the end points of the longest tracks in the selected events in the antineutrino-mode.

	CC0π	CC1π	CCOthers	NC	All
Reconstruction efficiency	85%	87%	91%	22%	68%

Table 4: Number of true interactions reconstructed. The purity and reconstruction efficiency of each true interaction is also shown.

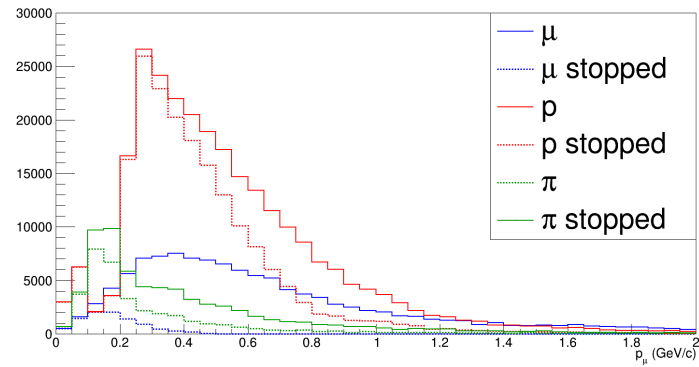


Figure 29: Momentum distribution of true particles in WAGASCI (plain) and corresponding distributions only for particles stopping into the WAGASCI module (dashed).

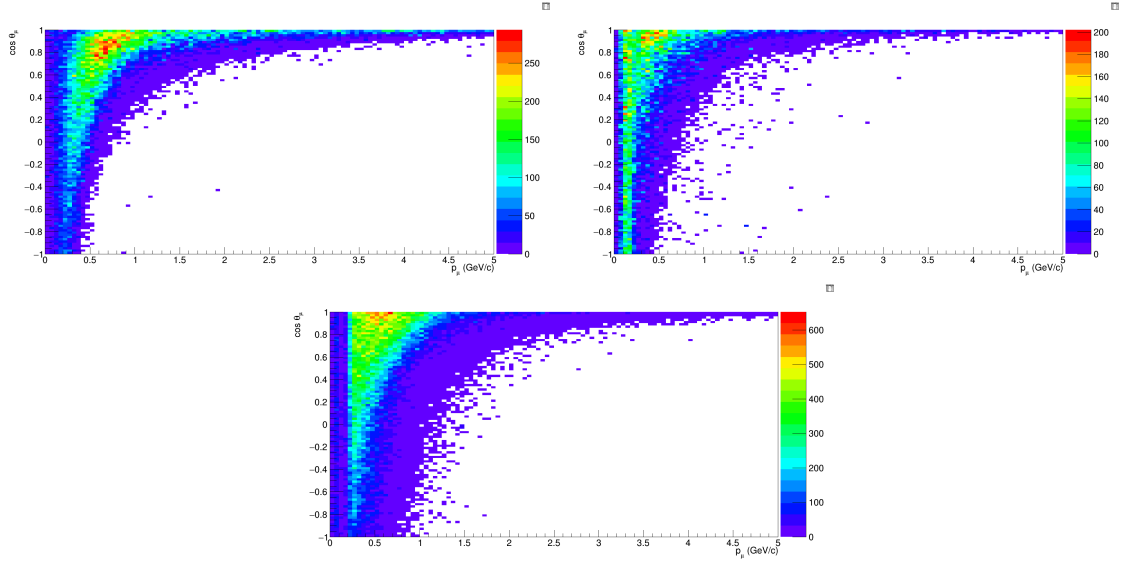


Figure 30: True number of muons (left), charged pions (right) and protons (bottom) in the two WAGASCI water-module as a function of the particles momenta and angles at 1.5° .

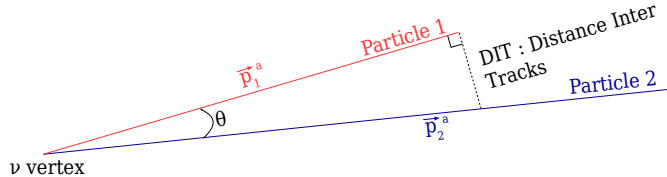


Figure 31: Definition of the distance inter tracks.

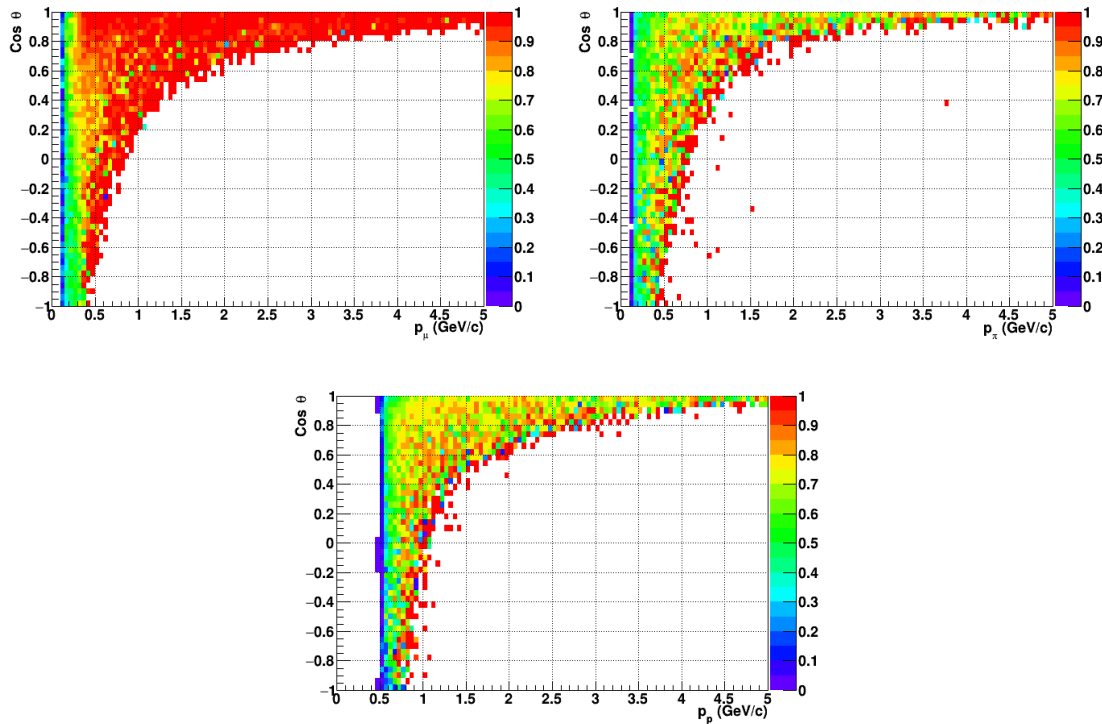


Figure 32: Reconstruction efficiency of muons (left), charged pions (right) and protons (bottom) in the WAGASCI water-module as a function of the particles momenta and angles.

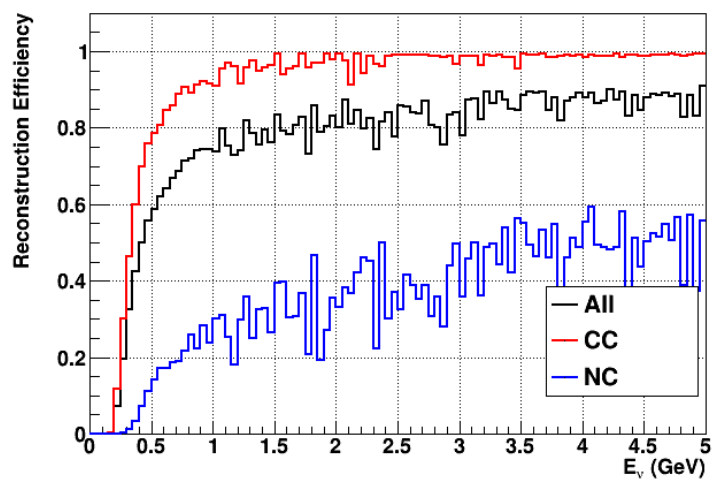


Figure 33: Reconstruction efficiency of all neutrino (black), CC (red) and NC (blue) interactions in the WAGASCI water-module as a function of the neutrino energy.

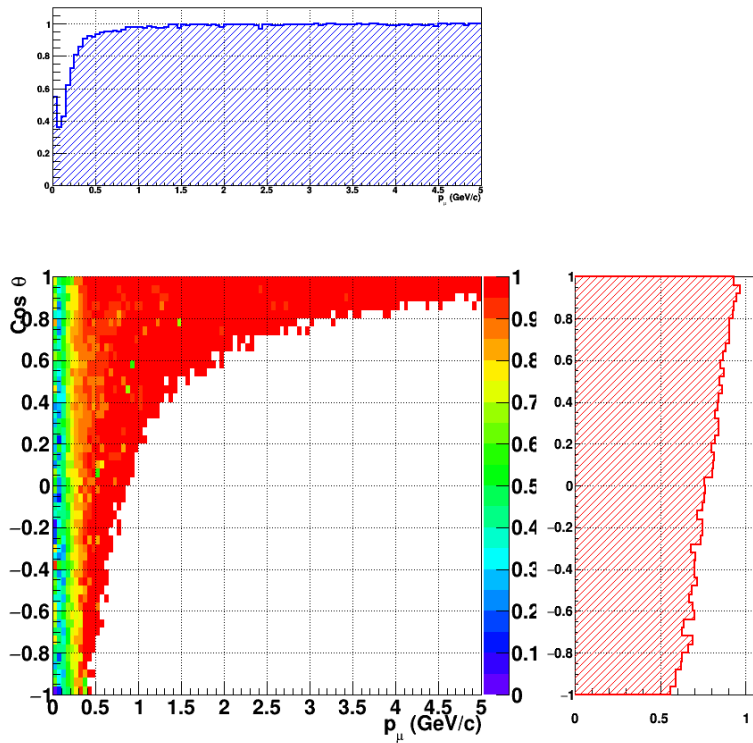


Figure 34: Reconstruction efficiency of CC interactions in the WAGASCI water-module as a function of the muon kinematic variables (momentum and angle).

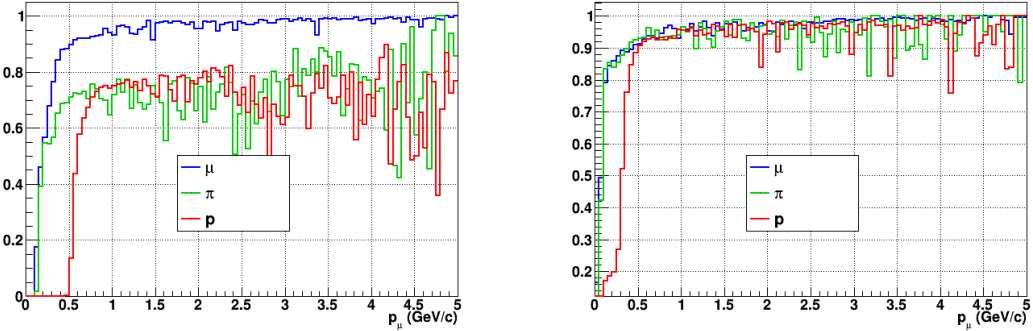


Figure 35: Reconstruction efficiency for muons, pions and protons in the water-in (left) and water-out (right) modules.

Note that a Particle Identification Algorithm has been also developed. It is based on the charge deposition of the particles in the scintillator, of the detection of a decay-electron. However, this information highly depends on the number of scintillator hit by a particle, which creates an important difference between a real WAGASCI module and the one used for the ND280-upgrade simulation. For this reason, the corresponding results will not be detailed here, but can be found in [?].

7.2 Background subtraction: the water-out module

In the nominal configuration, 20% of the neutrino interactions occurs on scintillators (C_8H_8). This background should be removed in order to measure the neutrino interaction on the same target as Super-K, which suppress the differences in cross-section models. For this purpose, we propose to use a water-out module, where the water is replaced by air. The detector is therefore fully active and has a 3 mm spatial resolution (scintillator thickness) which create an ideal detector to reconstruct and identify hadrons, and study np-nh interactions. The counter-part is the difference in particle energy deposition between the water and this water-out module that will need to be corrected for. In this section, we present the capabilities of such a module, and the impact it can have on cross-section measurements for the neutrino community in general and T2K in particular. The same reconstruction and selection as the water-in module is applied. Figure 35 shows the comparison between the water-in and the water-out reconstruction efficiencies for muon, pions and protons. 90% of the muons and 87% of the pions are reconstructed, while 70% of the protons are even reconstructed. It allows to lower down the proton threshold to 250 MeV/c (see Table 5).

As a consequence of tracking even low momenta particle, the reconstruction efficiency is uniform and almost maximal on the entire $\cos \theta_\mu$ phase space, as shown on Figure 36.

	μ	π	p
Reconstruction Efficiency Momentum threshold	90% 50 MeV/c	87% 50 MeV/c	70% 250 MeV/c

Table 5: Reconstruction efficiency, proportions of μ -like and non μ -like and momentum threshold for muons, pions and protons in the empty module. The threshold is defined as the maximal momentum for which particles have a reconstruction efficiency smaller than 20%.

576 Since the fiducial mass represents 0.25 tons, the total number of events is divided by a
 577 factor of 3 compared to the water-in module. The water-out module offers interesting
 578 possibilities to study np-nh interaction since 70% of the protons are reconstructed. In the
 579 future, a possible separation as a function of the number of proton track will be studied.
 580 Moreover, we are currently pursuing the use of single and double transverse variables (cite
 581 Xianguo) to open new possibilities for separating np-nh from Final State Interactions, or
 582 for isolating the interactions on hydrogen from interactions on carbon in this module.

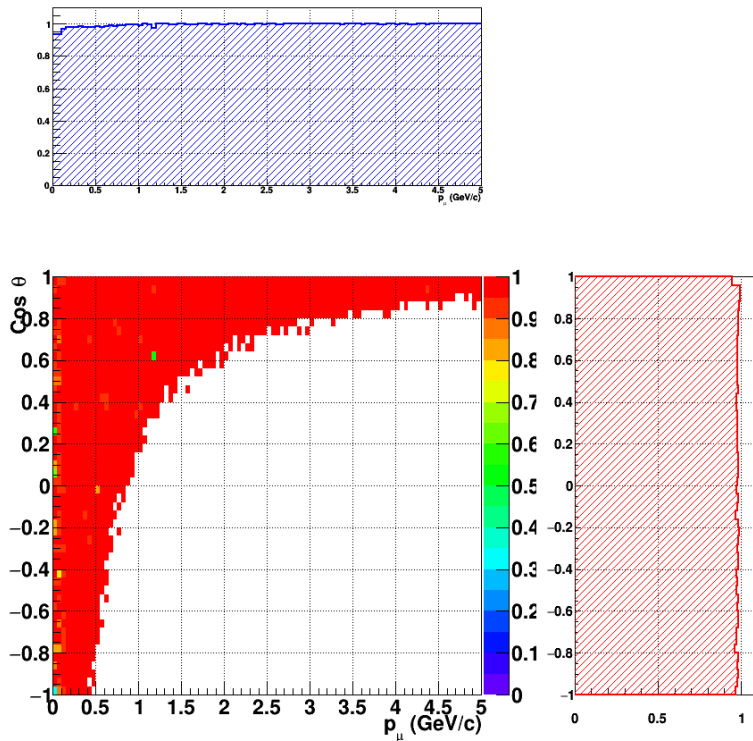


Figure 36: Reconstruction efficiency of CC interactions in the WAGASCI empty module as a function of the muon kinematic variables (momentum and angle).

583 **8 Schedule**

584 We would like to start a physics data taking from T2K beam time after the summer
585 shutdown in 2018. By then, commissioning and tests of the detectors will be completed
586 in J-PARC T59. The experiment can run parasitically with T2K, therefore we request no
587 dedicated beam time nor beam condition as discussed in the following section.

588 Once the approved POT is accumulated, the WAGASCI modules will be removed
589 from the experimental site, but we would like to keep the Baby-MIND and the Side-MRD
590 modules on the B2 floor of the NM pit as common platforms of future neutrino experiments
591 using the T2K neutrino beam.

592 **9 Requests**

593 **9.1 Neutrino beam**

594 The experiment can run parasitically with T2K, therefore we request no dedicated beam
595 time nor beam condition. As data taking periods, we request the ‘nominal’ T2K one-year
596 operation both for the neutrino beam and the antineutrino beam. The T2K has been
597 requesting 0.9×10^{21} POT/year and actually accumulating about 0.7×10^{21} POT/year in
598 recent years. For each year, starting from the Autumn, T2K is running predominantly in
599 the neutrino mode or in the antineutrino mode. Our request is to have one-year neutrino-
600 mode data and another one-year antineutrino mode data assuming that the POT for the
601 fast extraction in each year is more than 0.5×10^{21} POT.

602 **9.2 Equipment request including power line**

603 We request the followings in terms of equipment on the B2 floor:

- 604 • Site for the WAGASCI modules, Side-MRD modules and BabyMIND and their elec-
605 tronics system on the B2 floor of the near detector hall (Fig. 2).
- 606 • Anchor points (holes) on the B2 floor to secure the WAGASCI modules, Side-MRD
607 module and Baby-MIND (Fig. ??)
- 608 • Power line for the magnets in Baby-MIND: 400 V tri-phase 48-to-62 Hz, capable of
609 delivering 12 kW.
- 610 • Electricity for electronics and water circulation system, 3 kW, standard Japanese
611 electrical sockets.
 - 612 1. Online PCs: 2.1 kW
 - 613 2. Electronics: 0.7 kW
 - 614 3. Water sensors: ?

- 615 • Air conditioner for cooling heat generation at Baby-MIND magnets, online PCs and
616 electronics
- 617 • Beam timing signal and spill information
- 618 • Network connection

619 **9.2.1 Baby MIND Equipment request including power line**

620 We request the following in terms of equipment on the B2 floor:

- 621 • Site for the Baby MIND detector and its electronics systems on the B2 floor of the
622 near detector hall.
- 623 • Anchor points (holes) on the B2 floor to secure the 9 support frames, of order 4 holes
624 per frame, detailed floor plans to be communicated in a separate document.
- 625 • Power line for the magnet: 400 V tri-phase 48-to-62 Hz, capable of delivering 12
626 kW. We have a wish for the magnet power line to be installed and available to us by
627 beginning of March 2018.
- 628 • Electricity for electronics, 1 kW, standard Japanese electrical sockets.
- 629 • Beam timing signal and spill information
- 630 • Network connection

631 The infrastructure for much of the above exists already, and will be shared in part with
632 the WAGASCI experiment. Exceptions are the power line for the magnet and holes in the
633 B2 floor to anchor the detector support structures.

634 **10 Conclusion**